Measuring second-order time-average pressure

B. L. Smith and G. W. Swift
Condensed Matter and Thermal Physics Group, Los Alamos National Laboratory, Los Alamos, New Mexico 87545

(Received 21 February 2001; accepted for publication 2 May 2001)

Measurements of the spatial distribution of the time-averaged second-order pressure in a plane standing wave in atmospheric air are reported. Several measurement pitfalls are identified, and solutions are described. These include accounting for slight nonlinearity of the piezoresistive transducer and careful mounting of the transducer. Streaming causes extra complication when a capillary-connected manometer is used. With the proper technique and instrumentation, results are in good agreement with theory. © *2001 Acoustical Society of America.*
[DOI: 10.1121/1.1382615]

PACS numbers: 43.25.Qp, 43.25.Zx, 43.25.Gf [MFH]

I. INTRODUCTION

In thermoacoustic engines and refrigerators, streaming can transport a significant amount of heat. One initial attempt[1] to diagnose such streaming by measuring the second-order time-average pressure differences accompanying it was qualitatively reasonable but did not inspire high confidence in quantitative accuracy. Hence, we undertook the simpler measurements described here to learn how to measure second-order time-average pressure differences accurately and routinely.

For our purposes, a nonlinear periodic pressure wave can be described by

$$p(x,y,z,t)=p_m+\mathrm{Re}[p_1(x,y,z)e^{i\omega t}]+p_{2,0}(x,y,z)+\mathrm{Re}[p_{2,2}(x,y,z)e^{i2\omega t}]+\cdots. \quad (1)$$

The Eulerian pressure p, which is the pressure at a given location x,y,z as a function of time t, is written as the sum of several terms. The mean pressure p_m is the steady pressure that exists in the absence of any acoustic oscillation. It is usually independent of x,y,z, because body forces such as gravity are usually negligible. The fundamental acoustic oscillation at angular frequency $\omega=2\pi f$ is accounted for with the complex function $p_1(x,y,z)$, whose magnitude gives the amplitude of the fundamental pressure oscillation and whose phase gives the temporal phase of the oscillation. In the absence of nonlinear effects these p_m and p_1 terms might suffice. However, nonlinear effects, such as that described by the $(\mathbf{v}\cdot\nabla)\mathbf{v}$ term in the momentum equation (where $\mathbf{v}$ is the velocity), generate both harmonics such as $p_{2,2}$ and time-averaged phenomena such as streaming and the time-averaged second-order pressure denoted here by $p_{2,0}$. In our notation, the first subscript, 2, indicates that the magnitude of this term is second order in the acoustic amplitude, and the second subscript, 0, indicates the temporal frequency of the term. Measurement of $p_{2,0}$ is challenging because it is much smaller than both p_m and $|p_1|$.

The nature and magnitude of $p_{2,0}$ have generated activity and controversy in the acoustics literature. Twenty years ago, much of this activity was inspired by the desire to understand the radiation pressure on an acoustically levitated sphere. Decades earlier, the interest focused on the radiation pressure exerted by an ultrasonic beam on a flat plate. This body of work is reviewed by Lee and Wang,[2,3] who rightly point out that the confusion and controversy arise because radiation pressure is a small, subtle nonlinear effect, and in particular that extreme care must be taken to pose questions clearly. It is widely accepted[2–4] that

$$p_{2,0}=\frac{|p_1|^2}{4\rho_m a^2}-\frac{\rho_m|\mathbf{v}_1|^2}{4}+C, \quad (2)$$

if viscous and thermal effects can be neglected, where ρ_m is the mean density, a is the speed of sound, and C is a constant that is independent of space and time. For the plane standing wave of interest to us below, whose pressure amplitude is P_1 (a positive real number) at the pressure antinode $x=0$, the fundamental wave is described by

$$p_1(x)=P_1\cos kx, \quad (3)$$

and

$$|\mathbf{v}_1(x)|=(P_1/\rho_m a)|\sin kx|, \quad (4)$$

yielding

$$p_{2,0}=-\frac{P_1^2}{2\rho_m a^2}\sin^2 kx+C'. \quad (5)$$

Much of the historic controversy about radiation pressure has arisen from C (or C'), whose value depends on constraints external to the wave itself. For example, C depends on whether a resonator is vented to atmospheric pressure p_m at a particular location or is sealed with p_m trapped in the resonator before it is insonified. To avoid this confusion, we will consider only the difference between $p_{2,0}$'s measured at two different locations, so that the location-independent constant C is irrelevant. (The acoustic-levitation literature avoids this issue as well, because the net radiation force on a body completely enveloped by a sound wave is independent of C.) Our apparatus, described in Sec. II, had many pressure-sensor ports disposed along the standing wave, essentially allowing $p_{2,0}$ differences to be measured between ports. The experimental results, described in Sec. III, are in good agreement with Eq. (5).

However, to achieve these experimental results we had to avoid the many subtle pitfalls discussed in Sec. IV, only some of which we had anticipated. Some pitfalls depend on the hydrodynamics and acoustics of the wave and the wave-to-transducer fluid interface; others are characteristic of the particular transducer we used. The main purpose of this paper is to explain these pitfalls, so that other researchers can avoid them.

II. APPARATUS

The apparatus used in this study is shown schematically in Fig. 1. All measurements are made with 80-kPa air (atmospheric pressure at Los Alamos) inside of a 0.91-m-long aluminum pipe having an inner diameter of 10.2 cm. The top end of the pipe is closed by a plate that enforces a velocity node at this location. The flow entering the pipe at the lower, ''open'' end passes through a honeycomb flow straightener (10-cm-long, 4-mm-diameter tubes, with nearest neighbors separated by 0.25-mm-thick web) to ensure that no large turbulent structures enter the pipe and that the velocity profile is uniform. Pressure measurements are made at nine equally spaced locations (including the closed end) that extend down the entire pipe. The measurement ports are staggered azimuthally to prevent any disturbance created at one port from affecting another. The clean geometry is designed to create a plane standing wave as described by Eqs. (3) and (4) with $x=0$ at the closed end, and therefore a known distribution of p_1 and $p_{2,0}$.

The wave is generated by a driver system consisting of eight JBL 2206H loudspeakers. The speakers are arranged in four parallel sets of two speakers in series. This arrangement is capable of providing sufficient displacements and larger pressure amplitudes than are possible with all eight speakers in parallel. In order to allow for operation outside of the manufacturer's specifications for electrical power and frequency without thermal damage to the voice coil, the passive cooling system provided in each speaker by the manufacturer is replaced by the active system sketched in Fig. 1(b). The cooling flow loop is closed to ensure that no air is added or removed from the apparatus. Air driven by a blower is cooled by a heat exchanger before entering eight parallel paths, one to each speaker. The air enters the speaker through the center of the magnet, and is forced though the gap between the magnet and the voice coil. It then exits through the three ports in the magnet which originally provided passive cooling. These ports are connected to the inlet side of the blower, thus completing the cooling loop.

The fundamental resonance of the system is found to be $f=70$ Hz, with almost a quarter wavelength in the 0.91-m-long pipe. At this frequency, pressure amplitudes of 14 kPa (174 dB *re* 20 μPa rms) are easily achievable at the closed end. For the next resonance, at $f=210$ Hz, almost three-quarter wavelengths are in the pipe and a pressure amplitude of 7 kPa can be produced. The complicated geometry of the speakers' enclosure plus the pipe suppresses harmonic generation,[5] so shock waves do not occur even at these high amplitudes.

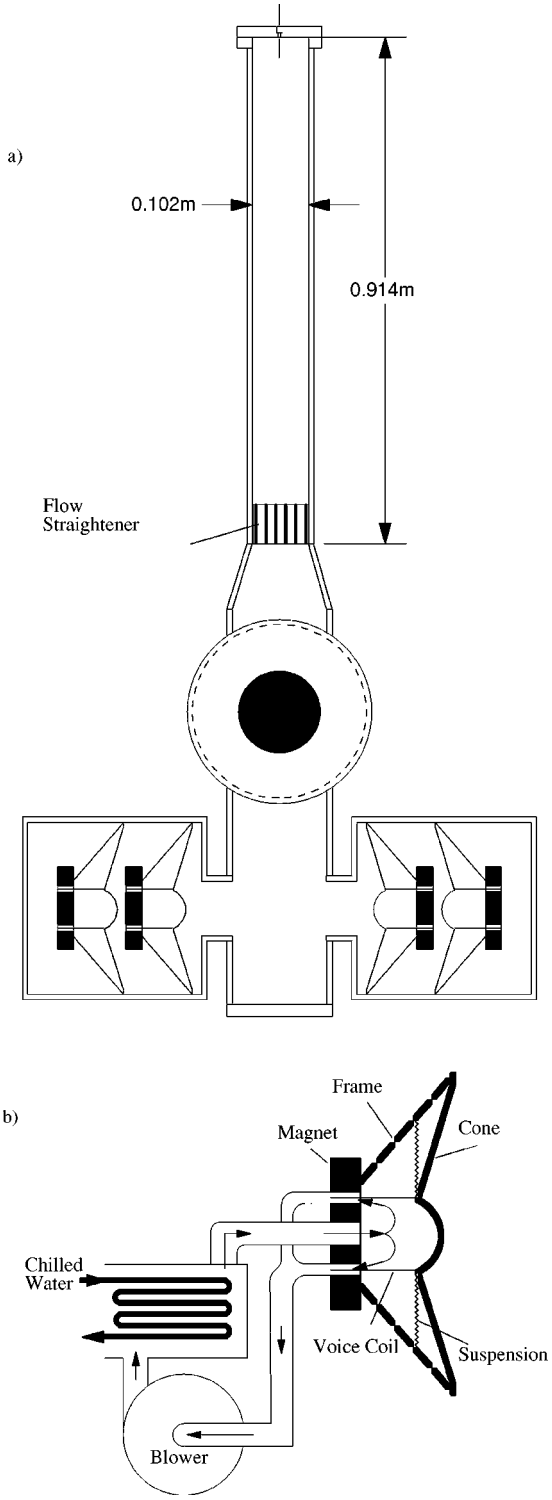

FIG. 1. Schematics of apparatus. (a) Pipe and driver system. Cross sections of four of the eight speakers are visible in the lowest part of the drawing; the other four have the same arrangement, but displaced upward along the apparatus and rotated 90° with respect to the long axis of the apparatus. (b) Detail of cooling-air loop for one speaker. The blower and chilled-water heat exchanger are shared among all eight speakers.

III. MEASUREMENTS OF $p_{2,0}$

All of the measurements reported in this section are made using differential piezoresistive pressure transducers (Endevco 8510B) referenced to atmospheric pressure. Each sensor is mounted by the manufacturer inside the tip of a

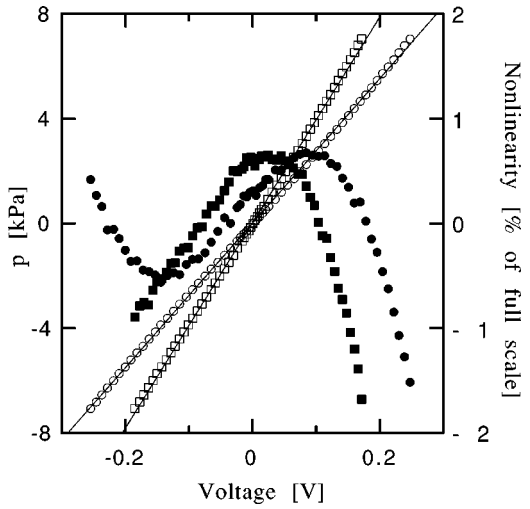

FIG. 2. Calibration data for two 1-psi pressure sensors. The raw data indicated by the open symbols and the linear fits to them are associated with the left axis. The filled symbols, associated with the right axis, show differences between the linear fits and the data.

3.86-mm-o.d. threaded tube. The threads begin above the sensor in an effort to reduce any strain on the sensor element when the transducer is torqued down. The transducer is sealed to the apparatus by an O-ring. Although these transducers are nominally linear (the manufacturer specifies less than 1% of full scale nonlinearity for the 1- and 2-psi transducers used here), their nonlinearity is significant for accurate measurements of $p_{2,0}$, so we account for it by in-house calibration of the transducers. The transducers are calibrated statically against a Bourdon-tube gauge (Wallace and Tiernan model FA 145, checked against a NIST traceable standard) with ticks of 27 Pa. The specified accuracy for this gauge is 33 Pa. The dial was read and recorded to an estimated accuracy of 13 Pa. The calibration data are shown in Fig. 2 for two 1-psi transducers (open symbols) along with linear fits to the data. The errors that would be incurred by using the linear fits are also plotted (closed symbols). Rather than the linear fit, we use a third-order polynomial to convert voltage to pressure. The differences between the data and the polynomial appear random with an rms value of 6 Pa, much smaller that the accuracy of the Bourdon-tube gauge. As will be shown in Sec. IV, failure to account for the nonlinearity of the pressure transducer would result in a substantial error in the time-averaged pressure result. The manufacturer's specifications for the piezoresistive pressure transducers give hysteresis and nonrepeatability errors that are each 0.2% of full scale. The rms sum of these two uncertainties plus the accuracy specification of the Bourdon-tube gauge is 0.6%, which will be assumed to be the uncertainty of the measurements.

For measurement of the time-dependent signals, data are acquired phase locked to the forcing signal by a 100-K sample/s 12-bit A-D acquisition system and stored on a laboratory computer. All results are averaged over at least 100 cycles. For each measurement, one transducer is placed in the closed end, while the second is successively moved along the other eight measurement ports. The voltage signals from the pressure transducers are converted to pressure $p(t)$ using the calibration curves described above before averaging. The

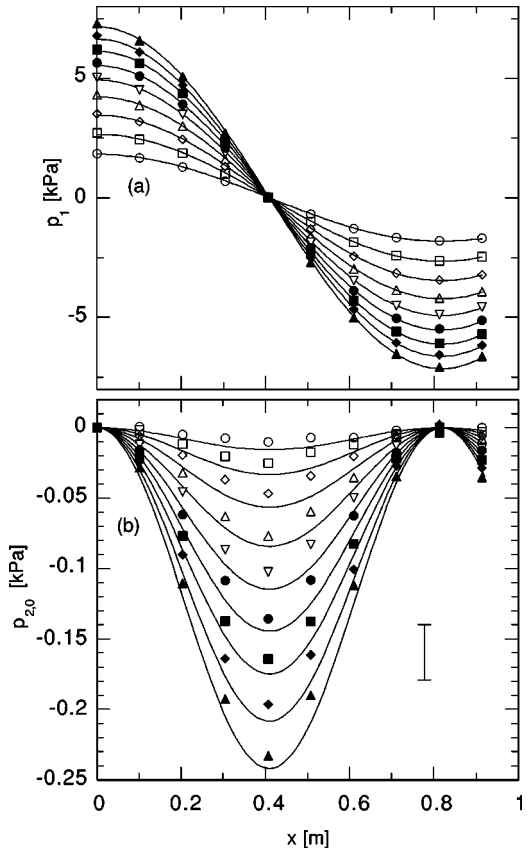

FIG. 3. Symbols show measured distributions of (a) $p_1(x)$ and (b) $p_{2,0}(x)$ for 210-Hz waves of nine different amplitudes in the pipe. In (a), the lines represent Eq. (3) with P_1 adjusted to fit the data. In (b), the lines represent Eq. (5) with no adjustable parameters, with P_1 obtained from the fits in (a), and with $C'=0$. A representative error bar is also shown.

fundamental pressure amplitude p_1 is calculated using a Fourier transform of $p(t)$, and the time average is also computed.

Two cases are studied: 210 Hz, for which two pressure antinodes exist within the measurement domain, and 70 Hz, which allows larger amplitudes. The 1-psi full-scale transducers are used for the 210-Hz case, while the 2-psi transducers are used for the 70-Hz case. In both cases, the largest amplitude studied is nominally the full scale of the transducer. Data are acquired as fast as the data acquisition system allows, resulting in 220 samples/cycle for the 210-Hz case and 700 samples/cycle for the 70-Hz case. The distribution of $p_1(x)$ and $p_{2,0}(x)$ are shown for these two cases in Figs. 3 and 4. In each case, data were acquired for several closed-end amplitudes P_1, and each amplitude is given a unique symbol. For each of the $p_1(x)$ distributions, the data are fitted to $P_1 \cos kx$, where P_1 is a fit parameter and $k = 2\pi f/a$. Recall from Sec. I that the theoretical distribution of $p_{2,0}$ contains a spatially independent constant that may vary with pressure amplitude. Since we are not interested in the absolute time-average pressure, but rather how this pressure varies in space, we ignore this constant by subtracting the time-averaged pressure at the closed end from each distribution. The results are shown in Figs. 3(b) and 4(b), along with curves generated using Eq. (5) and the P_1 values from

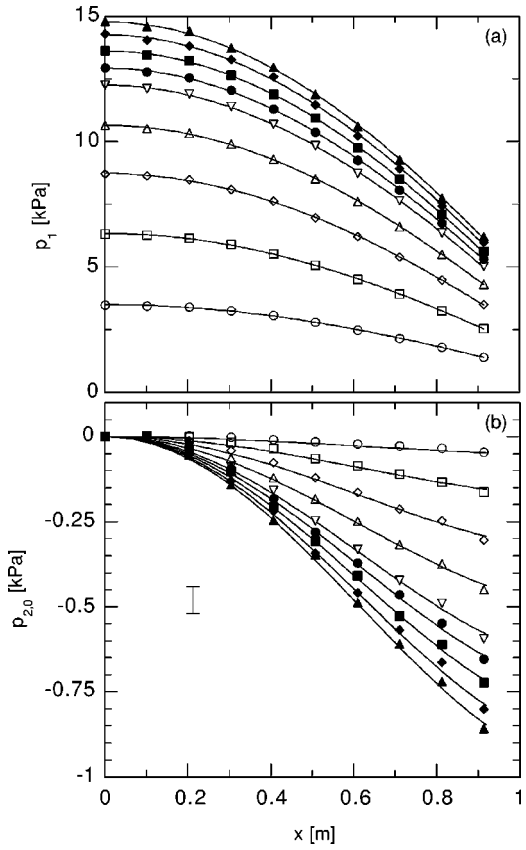

FIG. 4. Symbols show measured distributions of (a) $p_1(x)$ and (b) $p_{2,0}(x)$ for 70-Hz waves of nine different amplitudes in the pipe. In (a), the lines represent Eq. (3) with P_1 adjusted to fit the data. In (b), the lines represent Eq. (5) with no adjustable parameters, with P_1 obtained from the fits in (a), and with $C'=0$. A representative error bar is also shown.

the first-order curve fits. The $p_{2,0}$ distributions for 210 Hz shown in Fig. 3(b) match the theoretical distributions well, with differences everywhere less than the measurement accuracy. The agreement of the measurement with Eq. (5) is very good. A more accurate result can be obtained at higher amplitudes, such as the 70-Hz case shown in Fig. 4(b).

The writings of the theoretical leaders of a previous generation, such as Morse and Ingard[6] and Westervelt,[7] suggest that the truth of Eqs. (2) and (5) was once so well known that citation or publication of experimental validation was unnecessary. This attitude seems surprising, given the controversy in the literature mentioned above in Sec. I. Nevertheless, we have found only one previously published experimental $p_{2,0}$ result for a plane standing wave, similar to our Fig. 3: Van Doren's master's thesis.[8] His experiment is based on Morse and Ingard's suggestion to measure $p_{2,0}$ in a horizontal standing wave in air by observing spatial variations in the depth of a thin layer of water below the standing wave. Van Doren's results agree with the accepted theory to better than a factor of 2, but perhaps not as well as one would expect.

IV. PITFALLS

These results belie many possible pitfalls with the measurement of second-order time-average pressure, some of which have already been discussed briefly. In this section, the pitfalls that we have identified and therefore avoided will be discussed in detail.

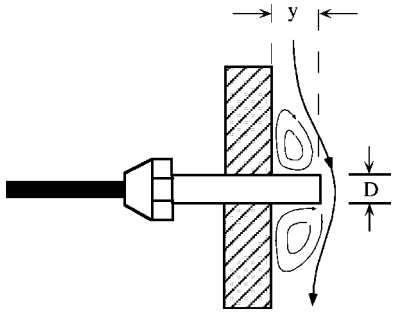

FIG. 5. Arrangement used to study the impact of pressure-sensor misalignment.

For steady flow, it is well known that a pressure sensor in the presence of fluid motion must be mounted flush to a wall that is parallel to the flow direction in order to provide an accurate measurement of Eulerian (static) pressure,[9] and that the pressure gradient normal to the wall is negligible.[10] However, the error incurred due to misalignment in an oscillatory flow is not known. For this reason, an additional pressure port was added to the apparatus at $x=0.864$ m that allowed the pressure sensor to be extended into the flow. The arrangement is shown schematically in Fig. 5. The sensor is traversed through the domain -1.3 mm$<y<1.3$ mm, where y is the extension of the sensor from the wall, by incrementally rotating the threaded transducer 1/6th of a turn resulting in increments of 0.13 mm in y. We estimate that y is known to within ± 0.13 mm. The maximum difference in alignment between the center of the sensor and its edges due to the curvature of the pipe wall is less than half of this estimated error. The speakers are driven at 70 Hz and the local velocity magnitude is estimated using Eq. (4) and the measured values of P_1 at the closed end. Data for five local velocities are shown in Fig. 6. In general, extending the sensor into the flow results in a negative pressure error that scales with $\rho|\mathbf{v}|^2$. The extension of the sensor from the wall is normalized by the sensor diameter D since we conjecture that three-

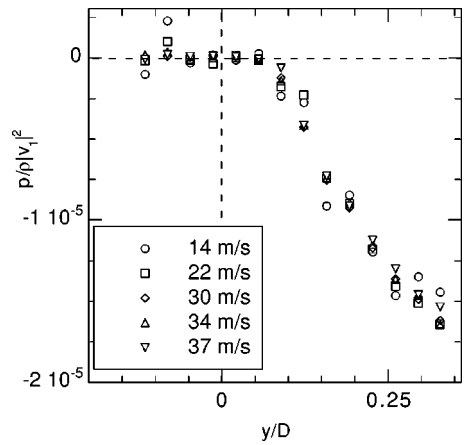

FIG. 6. Error in time-average static pressure measurement as a function of the sensor–wall alignment. Positive y values indicate that the sensor extends into the flow. Inset shows values of $|\mathbf{v}_1|$. Note that the normalization by $|\mathbf{v}_1|^2$ increases the scatter of the low-velocity data.

dimensional effects will begin to dominate as this value approaches 1, and the behavior may depart from $\rho|\mathbf{v}|^2$. The static pressure measurement error is caused by the pressure gradient associated with the streamline curvature induced by the obstacle (sensor) as shown in Fig. 5. No effect is seen until $y>0.05D$, which is not surprising given that the viscous penetration depth ($\delta_\nu=\sqrt{2\nu/\omega}$, where ν is the kinematic viscosity) for these conditions is $0.078D$. Interestingly, however, retracting the sensor inside of the pipe wall has no effect, at least up to $y=-1.27$ mm. With these results in mind, all measurements discussed in Sec. III were made with the pressure sensors recessed slightly from the inside wall of the pipe.

Although the results in Sec. III speak to the utility of the piezoresistive pressure transducer for simultaneous measurement of pressure amplitude and time average, other more sensitive devices for time-average measurements are available at a lower price. For example, a capacitance manometer with an uncertainty of 0.3% of the reading can easily be found. Furthermore, since the time-average pressure values are so small compared to the oscillation amplitudes, it is reasonable to expect that a great advantage in accuracy of the $p_{2,0}$ measurement could be obtained by utilization of a sensitive manometer. Even a simple water manometer, observed through a cathetometer, can easily resolve pressure differences of 0.1-mm $H_2O=1$ Pa. However, such devices are much less compact than their piezoresistive counterparts, and thus cannot be easily embedded directly in the wall of the apparatus. Typically, such devices are connected to a small ''tap'' in the wall of the apparatus via a flexible hose. It was anticipated that the acoustic impedance of the tap would need to be large to prevent the large acoustic pressure oscillations from causing large oscillatory velocity through the tap and therefore perhaps altering the reading. Despite our use of small-diameter taps, early results using this method indicated problems, so it was abandoned in favor of the piezoresistive transducers as described above. With confidence in the piezoresistive results, they now provide a baseline for comparison to illustrate problems encountered with the tap/remote manometer method.

In some measurements 6 years ago at Los Alamos, a 440-Hz standing wave in helium was used, with mean pressures ranging from 0.3 to 3 MPa and with two tap capillaries of 0.1-mm diameter and 1-m length extending from a differential manometer to two different places in the standing wave. Results bore little resemblance to Eq. (5). We have now identified two possible causes of error in this method: streaming in the capillary, and jetting at the capillary entrance.

Streaming occurs in the capillary because acoustic power $\mathrm{Re}[p_1\tilde{U}_1]/2$, where U_1 is the complex volume-velocity amplitude, must flow into and along the capillary to maintain viscous acoustic dissipation in it, and hence a term $\mathrm{Re}[\rho_1\tilde{U}_1]/2$ in the second-order time-averaged mass flux, with $\rho_1=\rho_m p_1/p_m$, must flow in as well. If the manometer has no leaks, no net mass can flow into the capillary, so $\rho_m U_{2,0}=-\mathrm{Re}[\rho_1\tilde{U}_1]/2$ must flow out of the capillary. Then, the second-order Navier–Stokes equation indicates that

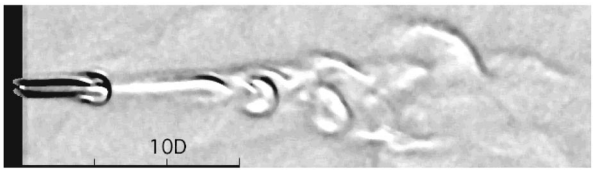

FIG. 7. Schlieren image of the flow induced when a pressure tap ($D=1.8$ mm) is exposed to an oscillating pressure. Pressure amplitude at the tap location is 0.51 kPa and $f=70$ Hz.

$\Delta p_{2,0}$ must exist in the capillary, in order to overcome viscous forces acting on $U_{2,0}$. The calculation of this $\Delta p_{2,0}$ is simple for a short capillary, treated as a lumped flow resistance R_ν, connected to an infinitely compliant manometer. In this case, $U_1=p_{1,e}/R_\nu$, where $p_{1,e}$ is the complex pressure amplitude at the capillary entrance. Then, $p_1(x)$ varies linearly along the length l of the capillary, from $p_{1,e}$ at the entrance to 0 at the manometer. Hence, $U_{2,0}$ is also linear, varying from $|p_{1,e}|^2/2p_mR_\nu$ at the entrance to 0 at the manometer. Integrating $\nabla p_{2,0}=\Delta p_{2,0}/\Delta x=U_{2,0}R_\nu/l$ along the length of the capillary yields

$$\Delta p_{2,0}=|p_{1,e}|^2/4p_m \tag{6}$$

for the pressure drop along the length of the capillary. Because $p_m=\rho_m a^2/\gamma$, where γ is the ratio of isobaric to isochoric specific heats, the error indicated by Eq. (6) is the same order of magnitude as the effect given in Eq. (5) that we are trying to measure. Remarkably, repeating this calculation for an infinite-length acoustic transmission line comprised of resistance per unit length and compliance per unit length gives exactly the same result. Including the effects of inertance and thermal relaxation present in a capillary whose diameter is not much smaller than the viscous and thermal penetration depths would presumably change the result. We have not verified Eq. (6) experimentally, but there seems to be no way to avoid such an effect if a capillary is used in an attempt to ''time average'' the pressure hydrodynamically.

Even if Eq. (6) (or its equivalent with inertance and thermal relaxation included) is accepted as true and is applied as a correction to measured results, jetting at the capillary entrance can sometimes add yet another second-order time-averaged pressure difference to the measurement. At Reynolds numbers much greater than unity, oscillating flow at the entrance to a tube is very asymmetric, with outflow creating a long jet (often with vortex rings) and inflow more broadly distributed in angle. This asymmetry of flow pattern causes asymmetry in the oscillating pressure drop across the entrance, so that the time-average pressure drop is nonzero. The magnitude of this pressure drop depends on details of the entrance edges, but its order of magnitude is $\rho|\mathbf{v}|^2$.

Details of one such jet are shown in the schlieren image taken in the vicinity of a pressure tap exposed to an oscillating pressure of amplitude 0.51 kPa shown in Fig. 7. A 1.8-mm-diameter 35-mm-long tap is used, and is connected to a 3.2-mm-i.d., 3.8-m-long hose. The pressure oscillations force air in and out of the pressure tap. The exiting air rolls into a vortex ring which propagates away under its self-induced velocity. The image clearly shows the roll-up of a nascent vortex ring and the starting jet behind the ring, which is

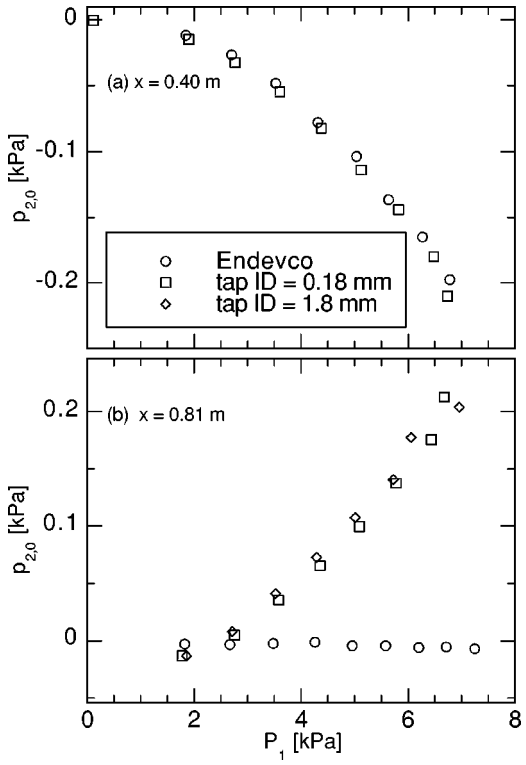

FIG. 8. Time-averaged pressure measurements made at 210 Hz using a capacitance manometer attached to a wall tap, compared with "correct" results using a piezoresistive transducer for both time average and amplitude. (a) Measurement at pressure node. (b) Measurement at pressure antinode.

indicative of a stroke length $2|\mathbf{v}_1|/\omega$ much larger than the orifice diameter. The remnants of rings from several previous cycles are also visible farther down stream. This type of flow is referred to as a synthetic jet, and it has been shown[11] that the pressure near the orifice of a synthetic jet is altered. Jetting is likely also occurring on the opposite side of the tap (into the flexible hose), resulting in a situation so complex that no resulting pressure measurement should be surprising or believed. Images were also acquired at higher frequencies and higher amplitudes and are not shown. In general, larger amplitude results in a longer stroke length and therefore a longer starting jet column. Increased frequency will reduce the stroke length and decrease the spacing between vortices. Note that the pressure amplitude used in Fig. 7 is very small compared with those used elsewhere in this study.

To assess the impact of this flow on pressure measurements, we used a capacitance manometer connected via the same hose to a 35-mm-long tap. Two tap diameters were used: 0.18 and 1.8 mm. As indicated above, we anticipated that this method would suffer most in regions of large pressure amplitude. For this reason, the speakers were driven at 210 Hz, and measurements were made at both the pressure node ($x=0.40$ m) and an antinode ($x=0.81$ m) and are plotted versus the closed-end pressure amplitude in Fig. 8. As expected, the pressure tap results are in good agreement with the piezoresistive transducer results at the pressure node [Fig. 8(a)]. However, where the pressure amplitude is large, at the pressure antinode [Fig. 8(b)], use of a pressure tap results in large errors that increase with pressure amplitude. It is also remarkable that the tap diameter seems to have little effect.

Other sources of error in the time-averaged measurement are due to effects within the transducer and how its output is interpreted. Although not of concern for these measurements, it is crucial to sample the signals rapidly enough to capture any short-duration features[1] that might contribute to $p_{2,0}$. Furthermore, if the transducer is nonlinear, measurement of its average voltage does not give the average pressure directly. Suppose that the transducer is exposed to pressure

$$p(t)=p_m+|p_1|\cos\ \omega t+p_{2,0}, \tag{7}$$

and that the transducer voltage depends on pressure via

$$V=V_m+A(p-p_m)+B(p-p_m)^2, \tag{8}$$

with B a small coefficient of nonlinearity. Substituting Eq. (7) into Eq. (8), taking the time average, and neglecting the very small term $Bp_{2,0}^2$ yields

$$V_{\text{avg}}=V_m+Ap_{2,0}+B|p_1|^2/2, \tag{9}$$

so that a naive measurement of average voltage would suggest that the average pressure is $p_m+p_{2,0}+B|p_1|^2/2A$ instead of the true value, $p_m+p_{2,0}$. For our calibrations of these transducers, B/A is found to be of the order of 0.005 kPa^{-1}.

In addition, it was found that for the more sensitive transducers used, the zero value was altered significantly each time the transducer was moved to a new port and torqued down. In fact, even though an effort was made to reproduce the same torque each time, the zero value of the transducer varied with a standard deviation of 0.03 kPa over the entire data set. For this reason, at each location, data were taken with the speakers off to obtain a correct zero value.

V. CONCLUSIONS

Accurate measurements of the second-order time-averaged pressure in a standing wave in atmospheric air have been made at two frequencies and at pressure amplitudes as large as 17.5% of p_m using piezoresistive pressure transducers built into the resonator walls. Several possible error sources are identified including sensor–wall alignment and transducer nonlinearity. It is found that the former error source can be eliminated simply by ensuring that the sensor is either flush or slightly recessed. Nonlinearity errors are removed by full calibration of the transducers, and the use of polynomial fits to the calibration data. It has also been shown that the use of capillary taps can lead to very erroneous results.

ACKNOWLEDGMENTS

The authors would like to thank C. Espinoza for his expert assistance in the construction of the driver system used in this work, M. Hamilton and S. Putterman for useful conversations, J. Olson for trying such measurements at Los Alamos 6 years ago, and the Office of Basic Energy Sciences in the U.S. DOE for financial support.

[1] S. Backhaus and G. W. Swift, ''A thermoacoustic-Stirling heat engine: Detailed study,'' J. Acoust. Soc. Am. **107**, 3148–3166 (2000).
[2] T. G. Wang and C. P. Lee, ''Radiation pressure and acoustic levitation,'' in *Nonlinear Acoustics*, edited by M. F. Hamilton and D. T. Blackstock (Academic, New York, 1998), pp. 177–205.
[3] C. P. Lee and T. G. Wang, ''Acoustic radiation pressure,'' J. Acoust. Soc. Am. **94**, 1099–1109 (1993).
[4] L. D. and E. M. Lifshitz, *Fluid Mechanics* (Pergamon, New York, 1982), Sec. 64.
[5] C. C. Lawrenson, B. Lipkens, T. S. Lucas, D. K. Perkins, and T. W. Van Doren, ''Measurements of macrosonic standing waves in oscillating closed cavities,'' J. Acoust. Soc. Am. **104**, 623–636 (1998).
[6] P. M. Morse and K. U. Ingard, *Theoretical Acoustics* (McGraw-Hill, New York, 1968), p. 869.
[7] P. J. Westervelt, ''The mean pressure and velocity in a plane acoustic wave in a gas,'' J. Acoust. Soc. Am. **22**, 319–327 (1950).
[8] T. W. Van Doren, ''Scattering of sound by sound in a waveguide, and d.c. pressure generation in a standing wave field,'' Master's thesis, The University of Texas at Austin (1990).
[9] F. M. White, *Fluid Mechanics* (McGraw-Hill, New York, 1986), p. 89.
[10] H. Schlichting, *Boundary-Layer Theory* (McGraw-Hill, New York, 1968).
[11] B. L. Smith and A. Glezer, ''The formation and evolution of synthetic jets,'' Phys. Fluids **10**, 2281–2297 (1998).